Functional Study of the Rat Cortical Microcircuitry with Voltage-sensitive Dye Imaging of Neocortical Slices

Rafael Yuste, David W. Tank[1] and David Kleinfeld[2]

Department of Biological Sciences, Columbia University, New York, NY 10027, [1]Biological Computation Research Department, Bell Laboratories, Lucent Technologies, Murray Hill, NJ 07974 and [2]Department of Physics 0319, University of California, La Jolla, CA 92093, USA

The computations performed within cortex are likely to be determined by its internal dynamics in addition to its pattern of afferent input. As a step toward characterizing these dynamics, we have imaged electrical activity in slices from rat primary visual cortex stained with the voltage-sensitive dye di-4-ANEPPS. In response to electrical stimulation two fluorescence signals of similar maximum amplitude are elicited. (i) A fast signal that peaks in a few milliseconds, is dependent on membrane voltage, and has a significant presynaptic component. This signal can be used to image electrical activity ratiometrically. (ii) A slow signal that peaks a few seconds after stimulation, does not reflect voltage changes, and may originate from changes in scattering properties of the slice and from interactions of the dye with the cells. The spatial pattern of fast signals obtained in response to focal stimulation of coronal slices is consistent with known interlaminar projection patterns. In tangential slices, imaging of fast signals reveals clustered horizontal responses. Finally, imaging of fast signals during epileptiform activation of the disinhibited circuit reveals propagating responses, without evidence for modular activation.

Introduction

The study of the function of the cortical circuitry has traditionally concentrated on mapping the afferent inputs and elaborating feedforward models to explain how receptive field properties are generated (Hubel and Wiesel, 1977; Gilbert and Wiesel, 1985; Chapman *et al.*, 1991). Recently, the field of attractor neural networks has kindled a resurgence of interest in the importance of the internal dynamics for neuronal computations (Hopfield, 1982). In these types of distributed circuit models the role of the feedback is pre-eminent and the dynamic trajectory of the electrical activity of the network becomes the computation itself (Hopfield and Tank, 1986). Thus, those internal dynamics, in concert with the pattern of inputs, could determine to a great extent the computations that occurs in neocortex (Georgopoulos *et al.*, 1989; Sompolinsky *et al.*, 1991; Ben-Yishai *et al.*, 1995; Douglas *et al.*, 1995; Somers *et al.*, 1995).

As a step towards characterizing the internal dynamics of neocortex we have imaged the responses of slices of rat visual cortex, stained with the voltage-sensitive dye (VSD) di-4-ANEPPS (di-4–6-amino-2-naphtyl-styryl-pyridinium), to different experimental paradigms. In principle, VSDs may enable simultaneous measurements of functional responses from many, or all, elements in the circuit. We chose the fluorescent styryl VSD di-4-ANEPPS because of previous biophysical studies of its responses (Fluhler *et al.*, 1985; Loew *et al.*, 1992) and used slices from rat visual cortex to experimentally access a well-studied cortical area while preserving most of its microcircuit. Optical recordings from extended areas were made with a charge coupled device (CCD) camera while high time resolution measurements at a single location were made with a photodiode.

We ask the following questions:

What Is the Biophysical Nature of di-4-ANEPPS Signals in Slices?

Previous work in slices has shown that VSDs can report transmembrane voltage changes (Grinvald *et al.*, 1982; Konnerth *et al.*, 1987). Yet there are also activity-dependent changes in the intrinsic optical properties of slices (Lipton, 1973; MacVicar and Hochman, 1991). Therefore it is important to understand the different contributions to the dye signal.

Can Information about the Circuit Diagram of Rat Visual Cortex be Revealed with Optical Imaging?

Anatomical techniques have been used to describe the pattern of axonal projections between different layers in cat and rat visual cortex (Gilbert and Wiesel, 1979; Burkhalter, 1989). In brief, projections from layer 4 to layer 2/3, from 2/3 to 5, from 5 to 6 and to 2/3, and from 6 to 4, as well as a system of clustered horizontal projections, have been described. We ask if these, and possibly other, projections may be observed from a functional perspective.

Is there Modularity in the Spontaneous Activation of the Network?

A central issue in understanding cortical circuitry is whether the cortex has a modular structure composed of iterated circuit elements (Mountcastle, 1982; Hubel and Wiesel, 1977). The existence of modular columns is controversial (Crick and Asanuma, 1986; Swindale, 1990) and part of this controversy stems from the lack of agreement of what constitutes a module. For this study, we define a module as a discrete unit with clear borders that is repeated several times in the circuit. In developing neocortex, repeated units with columnar shapes and discrete borders were discovered in rat neocortical slices by using calcium imaging (Yuste *et al.*, 1992). However, similar studies cannot yet be performed with the adult rat neocortex. We therefore ask if a modular organization in the adult rat neocortex could be revealed by imaging VSD signals in adult neocortical slice.

Preliminary results have been published in abstract form (R. Yuste, D. Kleinfeld and D.W. Tank, Society for Neuroscience Abstract, 1994).

Materials and Methods

Slice Preparation and Staining

Experiments were carried out with brain slices from visual cortex of Sprague–Dawley postnatal day 14–35 rats. Cortical areas 17 and 18a (Oc1M and B) were blocked according to Zilles and Wree (1985) and 400 μm thick coronal slices were cut using a vibratome (Microslicer DTK-1000) and kept in a submerged incubation chamber at room temperature (~22ºC). For some experiments tangential slices from visual and somatosensory cortex were cut. Normal artificial cerebro-spinal fluid (ACSF) contained (in mM) 124 NaCl, 5 KCl, 2 $CaCl_2$, 2 $MgSO_4$, 1.25 NaH_2PO_4, 26 $NaHCO_3$ and 10 dextrose, saturated with 95% O_2 and 5%

CO_2. A stock solution of 1 mg/ml di-4-ANEPPS (Molecular Probes, Eugene, OR) was made with 70% ethanol/H_2O. After 1–5 h in the incubation chamber, slices were transferred to a staining chamber, consisting of a small vial with an oxygen line, where they were stained in ACSF in which the stock solution of 4-ANEPPS was diluted to a final dye concentration of 0.01 mg/ml. After 15–30 min, labeled slices were placed in a submerged recording chamber mounted on the stage of a Zeiss IM35 inverted microscope (Newburg, NY). The recording chamber was kept at 33°C and perfused with heated ACSF. In some experiments the postsynaptic blockers D,L-5-amino-phosphonovaleric acid (APV, 100 μM: Sigma, St Louis, MO), 6-cyano-7-nitroquinoxaline-2,3-dione (CNQX, 20 μM: Tocris, Bristol, UK) and bicuculline methiiodide (BMI, 0.5–30 μM: Sigma) were included. Mg^{2+}-free experiments were done in ACSF without the addition of $MgSO_4$.

Imaging

Slices were placed in a recording chamber and were illuminated with a 12 V/100 W tungsten bulb powered by a constant-current power supply (Kepko, Queens, NY). We used 10 and 25 nm bandpass interference filters (Omega Optical, Bratleboro, VT), DCLP series dichroic mirrors (Omega Optical) and a f = 30 mm achromatic lens (Spindler-Hoyer, Milford, MA). Fluorescence was imaged using a CH220 cooled CCD camera (Photometrics, Tucson, AZ) with a Thompson 7882 UV enhanced chip. Camera frame rates were typically 10–15 Hz and each pixel was digitized at 12 bits. The spatial resolution was ~25 μm. Images were acquired, stored and analyzed using a Macintosh Quadra 800 (Apple Computers, Cupertino, CA) computer and custom software. Further analysis was carried out on a Sparc 2 workstation (Sun Microsystems, Mountain View, CA) using IDL (Research Systems, Boulder, CO). A single 818-UV photodiode (Newport, Irvine, CA), whose photocurrent was converted to voltage by a current preamplifier (Series 1211 Ithaco, Ithaca, NY), was used for single point measurements from regions ~200 μm in diameter. The voltage constitutes a measure of the baseline fluorescence intensity (F). The change in fluorescence intensity (ΔF) was measured by amplifying the output of the preamplifier with a second, AC-coupled amplifier (Series 113 Princeton Applied Research, Princeton, NJ), bandpass-filtered between 1 Hz and 3 kHz. The signal was sampled at 10 kHz using an A/D board (GW Instruments) and a Macintosh Quadra 800 computer.

Spectral Measurements

Absorption spectra of living slices stained with di-4-ANEPPS were measured using a diode array spectrophotometer (Hewlett Packard 8452A, Palo Alto, CA) and a custom made slice chamber that held the slice transversely and was filled with oxygenated ACSF at room temperature. The optical beam passed through a tangential slice cut from layers 2/3. To compensate for background scattering, we report the difference between spectra taken from stained versus unstained slices. Each data point is the average of over six positions in a slice. The fluorescence spectrum of di-4-ANEPPS was measured using stained coronal sections excited at λ = 500 (±5) nm. The fluorescence at 10 nm intervals was imaged with a photodiode that collected light from an ~1 mm diameter spot from the center of the slice; the light was bandpass filtered in a 6–8 nm interval (Omega Optical 10 nm bandpass interference filters, Brattleboro, VT). The measured intensity at each wavelength was corrected for the responsivity of the photodiode and the transmission coefficient and exact bandwidth of each filter according to:

$$\text{corrected value} = \text{measured value}/(H \times W \times T \times R)$$

where H is the height of transmission peak, W is the width of transmission peak, T is the transmission of the dichroic, and R is responsivity of the diode.

Electrophysiology

Local field potentials (LFPs) were recorded with glass micropipettes filled with ACSF or saline, with DC impedances of ~1 MΩ. The signal was sequentially fed into an amplifier (Neurodata model IR-283, New York, NY) and a preamplifier (Ithaco 1201) in DC mode and digitized using an A/D board and a Macintosh Quadra 800 computer. Temporal registration between images and electrophysiology was obtained by recording TTL pulses signaling the beginning and end of each CCD exposure with the electrophysiological record. Slices were stimulated with 25 μm, polyimide-coated tungsten electrodes (California Fine Wire, Pasadena, CA) in a bipolar configuration, using brief shocks of DC current. Statistical values are reported as mean ± standard deviation of the mean.

Table 1
Guide to layer boundaries in adult rat visual cortex

Layer boundary	Distance from pial surface (μm)
Pia to 1	0
1 to 2	~130
3 to 4	~500
5 to 6	~600
6 to white matter	~1400

Layer Determination

Layer boundaries were determined for a select number of slices by counterstaining with cresyl violet (e.g. Fig. 7). Otherwise, layers were determined by direct examination of the fluorescence staining pattern of di-4-ANEPPS, which stains heavily layers 2/3 and 5, leaving layers 1 and 4 relatively less stained. Finally, for slices where layers were difficult to judge, we used the distance from the pial surface as the ultimate criteria for where the layer boundary was located (Table 1).

These numbers result from our previous measurements and are compatible with other estimates from the literature (Zilles and Wree, 1985; Burkhalter, 1989; Langdon and Sur, 1990).

Results

Di-4-ANEPPS Preferentially Labels the Cortical Neuropil

The staining of a preparation with a VSD does not guarantee that the optical signals measured are related to changes in membrane potential (Grinvald *et al.*, 1988). To characterize the nature of the optical signals in our preparation, we first investigated which cellular structures were labeled under our staining conditions by imaging di-4-ANEPPS-stained slices with two-photon laser scanning fluorescence microscopy (Denk *et al.*, 1990; Fig. 1). This technique allows high-resolution imaging of structures located inside highly scattering media like the neocortex (Denk *et al.*, 1994).

Incubation with di-4-ANEPPS labeled strongly the cortical neuropil (up to 240 times increases in fluorescence over unlabeled slices), while areas containing somata and primary dendrites appeared less labeled (Fig. 1*A*). The average fluorescence intensity of the neuropil was ~2–4 times larger than an area covering somata and primary dendrites. Higher-magnification imaging demonstrated distinct staining of cytoplasmic membranes of neurons (Fig. 1*B*), nuclear membranes (arrow in Fig. 1*B*) and some intracellular organelles. The internalization occurred rapidly (within 20 min of the staining) and did not seem to change over the course of our experiments (up to 2 h). In the neuropil different structures could be tentatively identified as presynaptic terminals, glial cells, blood vessels, axons and dendrites. These staining patterns demonstrate that in cortical slices bath application of di-4-ANEPPS labels heterogeneous structures in the neuropil and that the dye is not restricted to the outer leaflet of the plasma membrane, becoming internalized.

Electrical Stimulation Produces a Fast, Voltage-related Signal and a Slow Signal of Complex Nature

Electrical stimulation of stained slices produced a reduction in

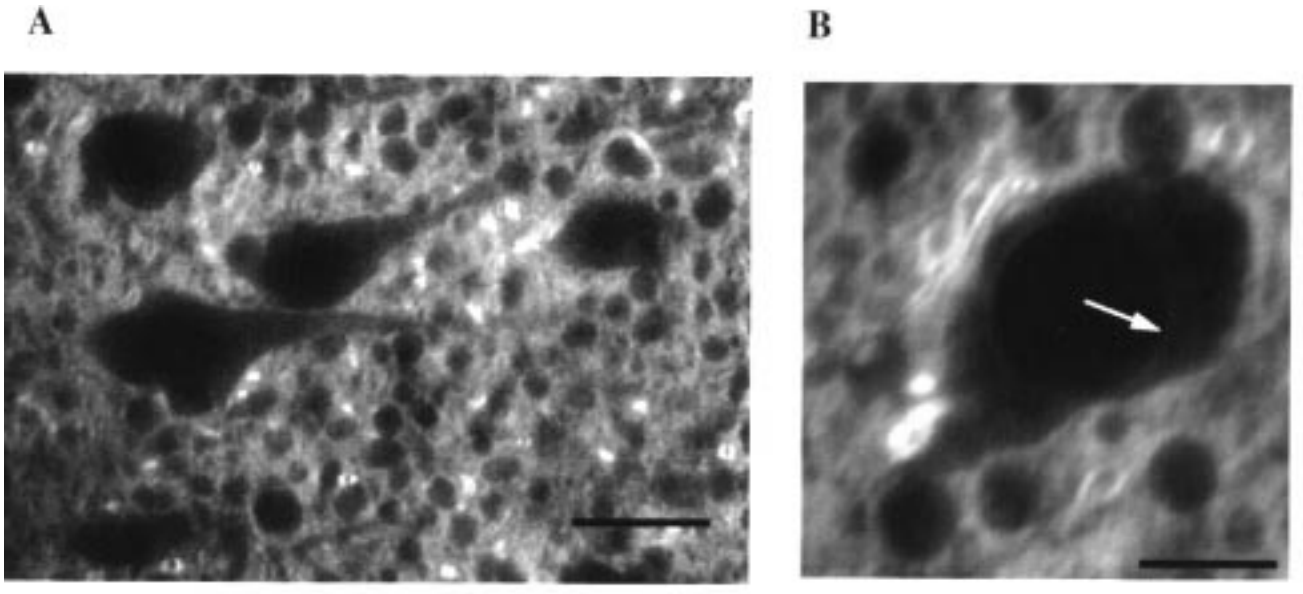

Figure 1. Di-4-ANEPPS stains the neuropil of neocortical slices and labels nuclear membranes. (*A*) Two-photon excitation fluorescence imaging of a coronal slice from rat primary visual cortex stained with di-4-ANEPPS. The cortical neuropil is strongly stained whereas somata and primary dendrites from pyramidal neurons are less stained. Many small round structures, possibly glial cells, can be distinguished. Scale bar = 40 μm. (*B*) Higher magnification of a two-photon image of the cell body of a pyramidal neuron from the same slice. The nuclear membrane is stained (arrow), demonstrating dye internalization. Scale bar = 20 μm.

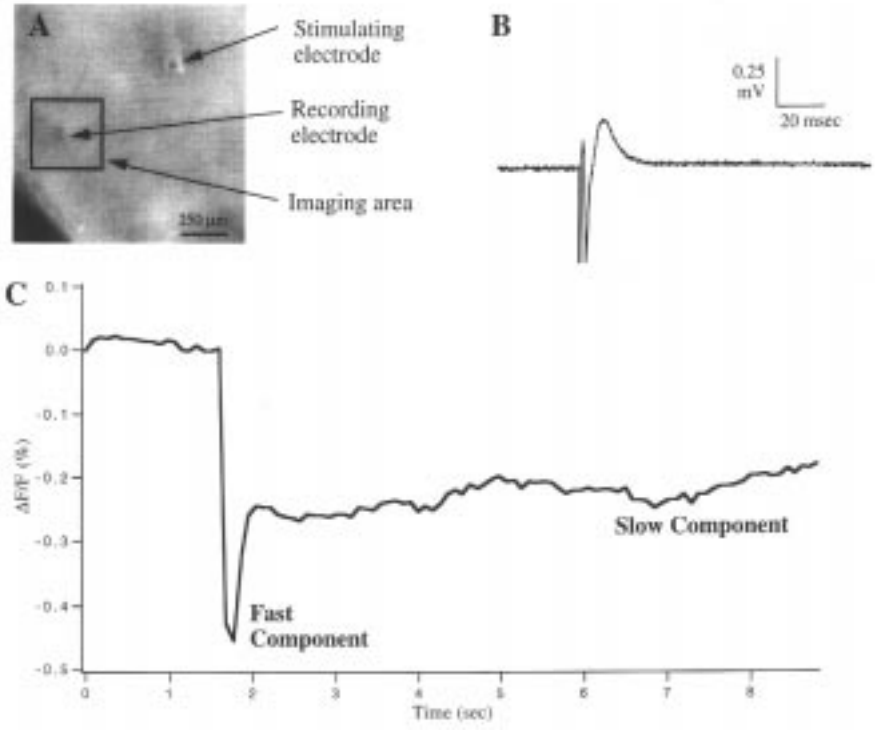

Figure 2. Electrical stimulation of a neocortical slice produces fast and slow signals. Imaging of the fluorescence response produced by a single electrical shock in a slice. (*A*) Orientation of the slice: pial surface is at the bottom left, layer 6 at the top right. A stimulation electrode was placed in layer 5 and optical (square) and electrical recordings were collected from layer 2/3. (*B*) Field potential, average of eight measurements. A 300 μs shock in layer 5 produces a biphasic field potential response. (*C*) CCD recording, average of eight measurements. The fluorescence in the area defined by the box was measured using 550 nm excitation and 600 nm long-pass emission filters. In response to a single electrical shock in layer 5, a decrease in fluorescence ($\Delta F/F$) is produced, which has a fast (tens of milliseconds) and a slow (seconds) time course.

the fluorescence signal with two clear temporal components (Fig. 2). In response to a single 300 μs electrical shock in layer 5, the photodiode signal measured in layer 2/3 had a 'fast' component that peaked within 10 ms of the onset of stimulation (Fig. 4*A*,*B*). In CCD images the fast component encompassed one or two frames (Fig. 2*B*,*C*) and is seen to merge into a 'slow' signal that peaked ~500–1000 ms from the time of stimulation; this slow signal was not correlated with changes in the LFP. For single shocks, both the fast and slow signals had similar amplitudes, $\sim\Delta F/F$ = 0.1–1% for optimal wavelengths (Fig. 2*C*). The noise in

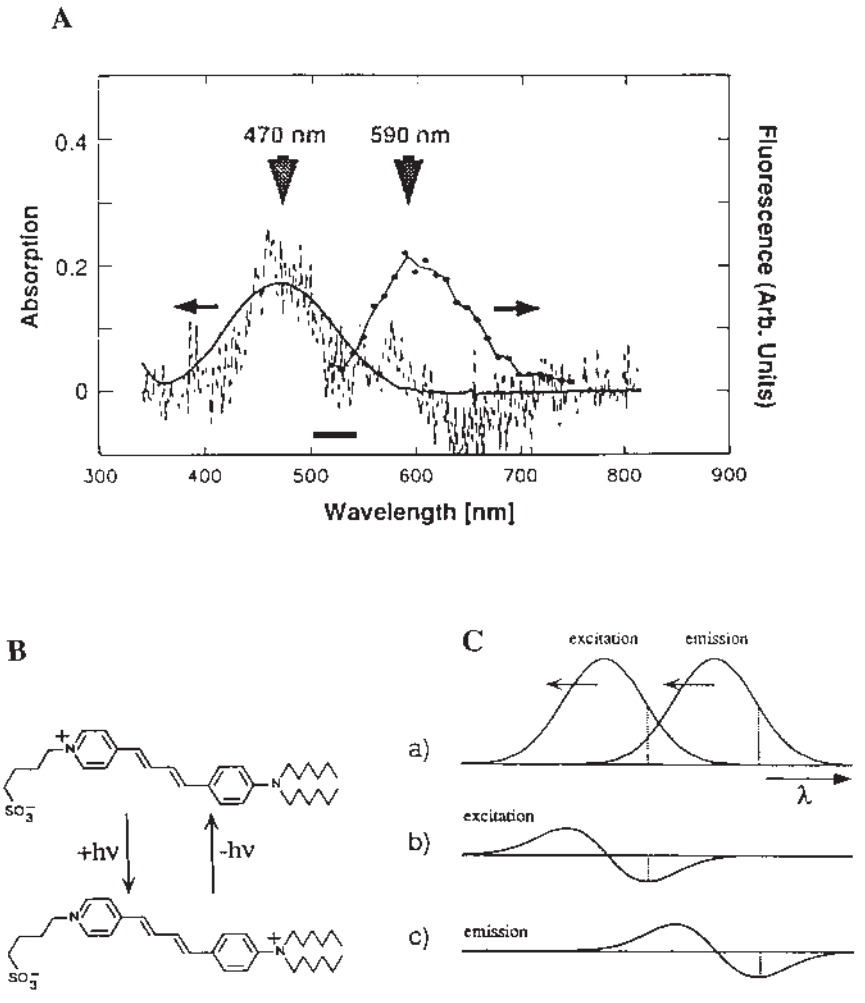

Figure 3. Absorption and fluorescence spectra of a living slice stained with di-4-ANEPPS and predictions from electrochromic theory. (*A*) Spectra measured from a tangential slice cut from layers 2/3 and stained with di-4-ANEPPS. Left curve: the stippled line represents the absorption spectrum from a slice. For comparison, the solid line shows the absorption spectrum from a solution of the dye. Both spectra peak at ~470 nm excitation. Right curve: fluorescence spectrum of the slice, which peaks at 590 nm. (*B*) Electrochromic behavior of a charge-shift probe. Left panel: formula of the similar styryl VSD RH-423, illustrating the charge shift that occurs with absorption of a photon. A similar mechanism has been postulated for di-4-ANEPPS (Loew *et al.*, 1979). The delocalized positive charge moves from the pyridinium nitrogen to the amino nitrogen next to the alkyl chains, which are presumably anchored in the plasma membrane. (*C*) During depolarization of the membrane, the energy of the excited state is raised and (a) the membrane depolarization thus shifts both the excitation and emission spectra to the blue; this produces biphasic action spectra (b, c). Exciting at the peak of the absorption, the predicted behavior of an electrochromic mechanism would therefore be a strong wavelength dependency of the emission (c), with a zero crossing point at the peak of the emission (diagram courtesy of C.-B. Chien).

unaveraged cCCD measurements was ~0.05% $\Delta F/F$ so the signal-to-noise ratio varied from 2 to 20. For multiple shocks, however, the slow signal grew by summation and eventually dominated in amplitude because of its slow decay (not shown).

To understand the nature of the signals we first characterized the absorption and fluorescence spectra of di-4-ANEPPS in living slices stained with the dye (Fig. 3*A*). The absorption spectrum of di-4-ANEPPS in stained slices peaked at λ = 470 nm (broken line) and was essentially identical to that of the dye in free solution (solid left line). The fluorescence spectrum showed a peak at λ = 590 nm (solid right line). Both absorption and fluorescence spectra are similar to those previously published from stained lipid vesicles (Montana *et al.*, 1989).

A feature of styryl VSDs is that the excitation and emission spectra are shifted in wavelength by a change in membrane potential (Fig. 3*B*,*C*), as opposed to a change in absolute absorption or fluorescence. For dyes with large dipole moments, like di-4-ANEPPS, this shift is expected to be linear with the change in potential, following electrochromic theory (Platt, 1956; Loew *et al.*, 1979; Montana *et al.*, 1989). To test if the fast signal represented a true membrane potential signal, we measured its wavelength dependency by using an excitation wavelength that corresponded to the peak of the absorption spectrum (λ = 470 nm) and varying the wavelength of the fluorescence emission collected. In response to a single 300 μs electrical shock in layer 5, the fast optical signal measured in layer 2/3 reversed in sign with increasing emission wavelengths, showing a crossover point at 590 nm (Fig. 4). Thus, shorter emission wavelengths produced an increase in fluorescence intensity (Fig. 4*A*) while longer wavelength produced a decrease (Fig. 4*B*). The zero crossing point (λ = 590 nm) and sign of the changes agree well with the derivative of the fluorescence spectrum; this suggests a first-order Stark effect (Fig. 4*C*, compare with Fig. 3*C*). This behavior mimics the blue-shift produced in the emission spectrum of voltage-clamped lipid bilayers stained with di-4-ANEPPS (Fluhler *et al.*, 1985). We concluded that the fast response of the dye is directly sensitive to membrane potential.

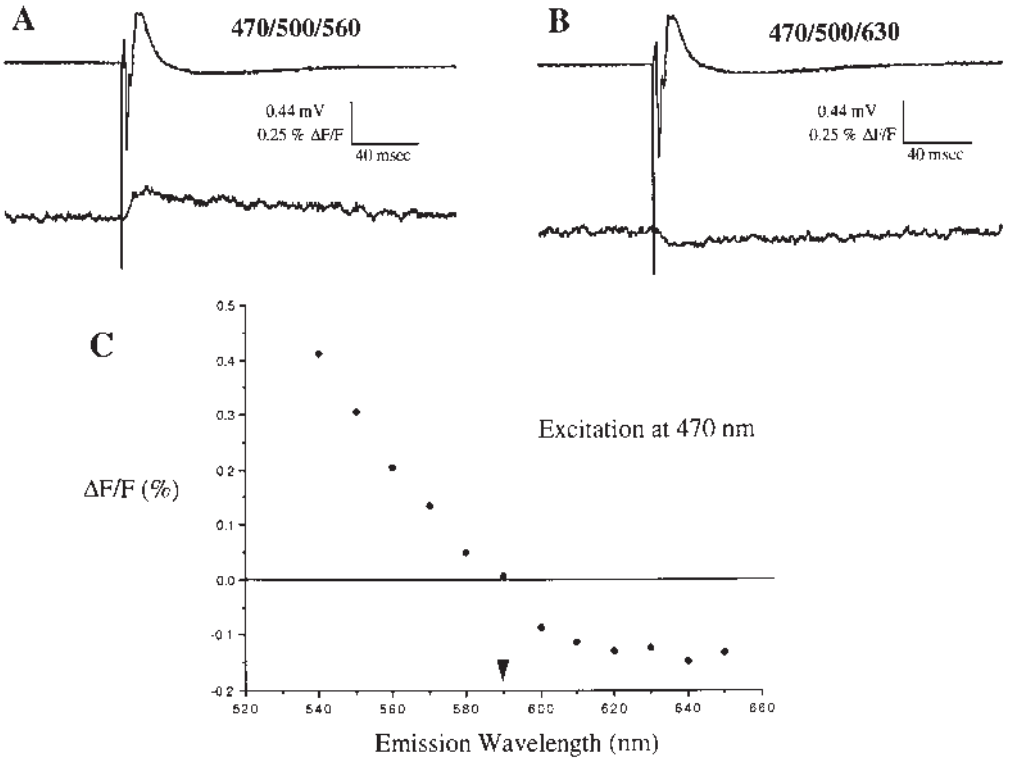

Figure 4. The fast signal shows a strong dependence on emission wavelength. (*A*) Combined field potential (top traces) and photodiode (bottom traces) measurements from layer 2/3 of a slice stimulated with a single shock in layer 5. The excitation filter was centered at 470 nm, the dichoic mirror at 500 nm and the emission filter at 560 nm. (*B*) A change of the emission wavelength from 560 nm (A) to 630 nm (B) changes the sign of the fluorescence response. (*C*) Graph of the $\Delta F/F$ versus emission wavelength measured at the peak of the fast signal, ~10 ms after the stimulus. Each point is the average of 16 measurements. The zero crossing occurs near 590 nm corresponds to the peak of the fluorescence spectrum (right curve, Fig. 3*A*).

In contrast to the fast signal, the slow signal showed no wavelength dependency (Fig. 5), indicating that it does not directly depend in changes of transmembrane potential. We used this lack of wavelength dependency to isolate the slow signal by imaging the fluorescence at λ = 590 nm, the zero crossing point for the change in emission, thus optically canceling the fast signal (bottom, Fig. 5*C*). We also isolated the fast signal by taking the ratio of the emission at either side of the emission peak (top, Fig. 5*C*). To investigate the mechanisms responsible for the slow signal we measured changes in reflectance produced by our stimulation paradigms in unstained slices. As previously described (Lipton, 1973; Grinvald *et al.*, 1982; Konnerth *et al.*, 1987; MacVicar and Hochman, 1991), electrical stimulation of unstained slices produced an decrease in light scattered in the forward direction. This signal peaked ~500 ms from the time of stimulation and decayed with a time course of several seconds (not shown). The sign of the reflectance changes and the similarity of the time courses suggests that most of the slow fluorescence signal seen in slices stained with di-4-ANEPPS may be due to changes in scattering properties of the slice.

Fast Signals Reflect Pre- and Postsynaptic Responses

To inquire what type of voltage changes constituted the fast signal, we measured with a photodiode the fluorescence changes produced in layers 2/3 in response to stimulation of layer 5 in the presence or absence of postsynaptic blockers.

Single shocks to layer 5 produced an optical signal in layers 2/3 that peaked ~10 ms after the stimulus. Simultaneously, field potentials from the same area showed clear pre- and postsynaptic components (Fig. 6*A*). Bath application of APV (100 μM) and CNQX (20 μM) abolished the postsynaptic response in the field potential without affecting the presynaptic volley (top trace, Fig. 6*B*). During this time, a reduction (35 ± 10%, n = 3 slices) in the peak optical signal was observed (bottom, Fig. 6*B*). After washing out the drugs, the field potential and optical response recovered their initial characteristics (Fig. 6*C*). These results indicate that fast VSD signals result from a combination of pre- and postsynaptic components.

The fast signal remaining under APV/CNQX could be caused by orthodromic activation of presynaptic terminals from layer 5 axons that project to layer 2/3 or by antidromic activation of somata and dendrites from layer 2/3 cells that project to layers 5, because extracellular stimulation of a cortical slice can activate both orthodromic and antidromic pathways. To explore if there could be a presynaptic component in VSD signals in slices, we recorded optically in the stratum radiatum of CA1 field of the hippocampus while stimulating the Schaffer collaterals, an experiment that precludes an antidromic activation of CA1 neurons because CA1 pyramidal neurons do not project back to the radiatum. In agreement with a previous report (Grinvald *et al.*, 1982), perfusing APV/CNQX led to a reduction (25 ± 15%, n = 4 slices) of the optical signal in the radiatum while completely blocking postsynaptic field potentials. The persistence of a fast signal in CA1 in the presence of synaptic blockade demonstrates that an orthodromic presynaptic signal can contribute significantly to VSD signals in brain slices, and suggests that after layer 5 stimulation the majority of the fast response seen in layer 2/3 could be mediated by orthodromic activation of layer 5

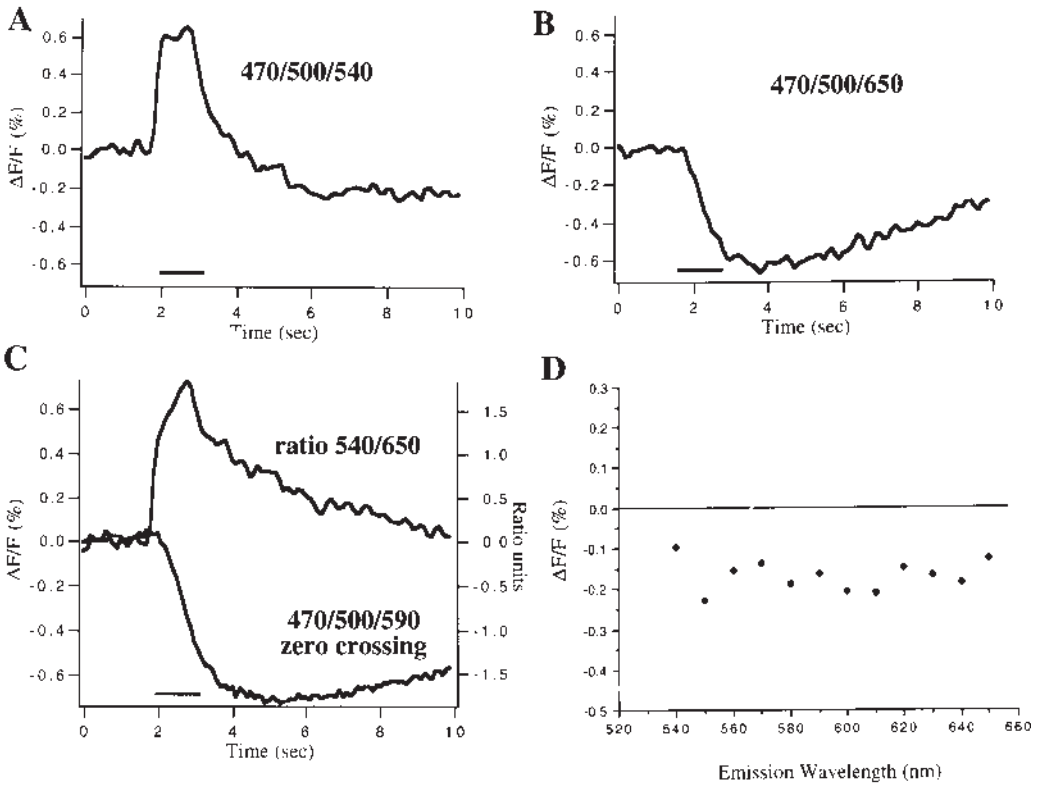

Figure 5. The slow signal is wavelength independent and can be isolated at the emission zero crossing point, while the fast signal can be isolated ratiometrically. (*A–C*) Fluorescence response from layer 2/3 of a slice stimulated with a 10 Hz, 1 s long train in layer 5. Each trace is the average of eight measurements. A fast signal can be detected that reverses sign when the emission filter is changed from 540 (*A*) to 650 nm (*B*). Notation of filter wavelengths is excitation/dichroic/emission. (*C*) Isolation of slow and fast signals. The slow signal is isolated at the emission zero crossing for the fast signal (bottom). The fast signal is isolated by taking the transient part of the ratio of responses at either side of the emission peak (e.g. 540 and 650 nm). (*D*) Graph of the $\Delta F/F$ versus emission wavelength, measured 21 s after the stimulus.

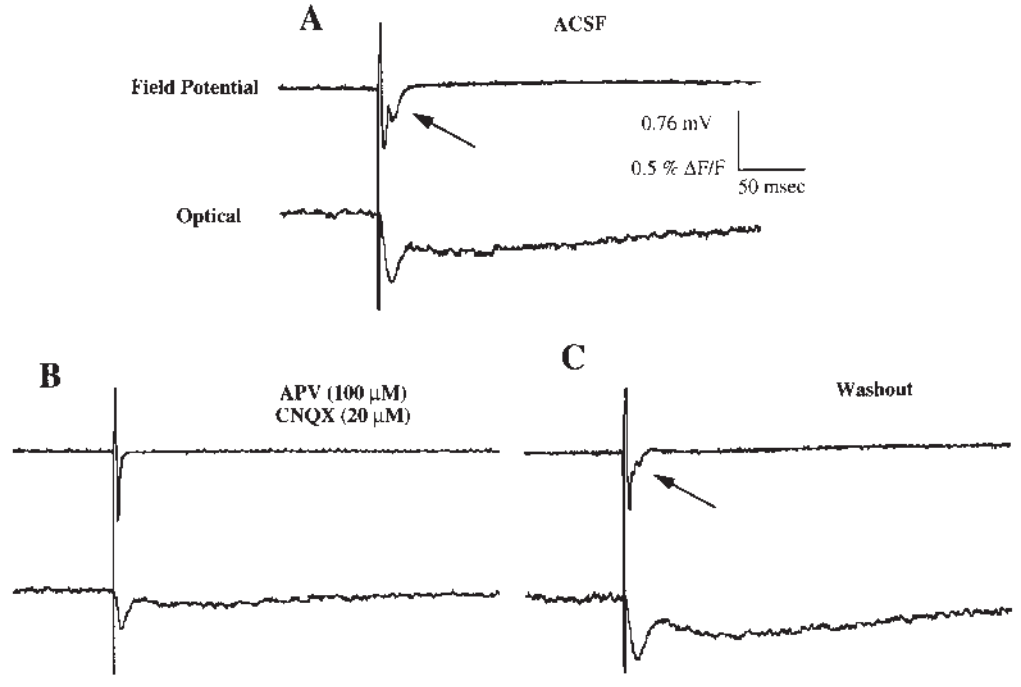

Figure 6. A major component of the fast signal is presynaptic. (*A*) Combined field potential (top) and photodiode (bottom) recordings from layer 2/3 of a slice stimulated with a single shock in layer 5. The fast signal peaks ~10 ms after the stimulus, concomitantly with the field potential changes. The slow signal was filtered in this experiment. (*B*) In the presence of APV (100 μM) and CNQX (20 μM), the postsynaptic field potential response (arrow) disappears, but the optical signal is still present, although with reduced amplitude. (*C*) The effect is reversible after washing out the drugs.

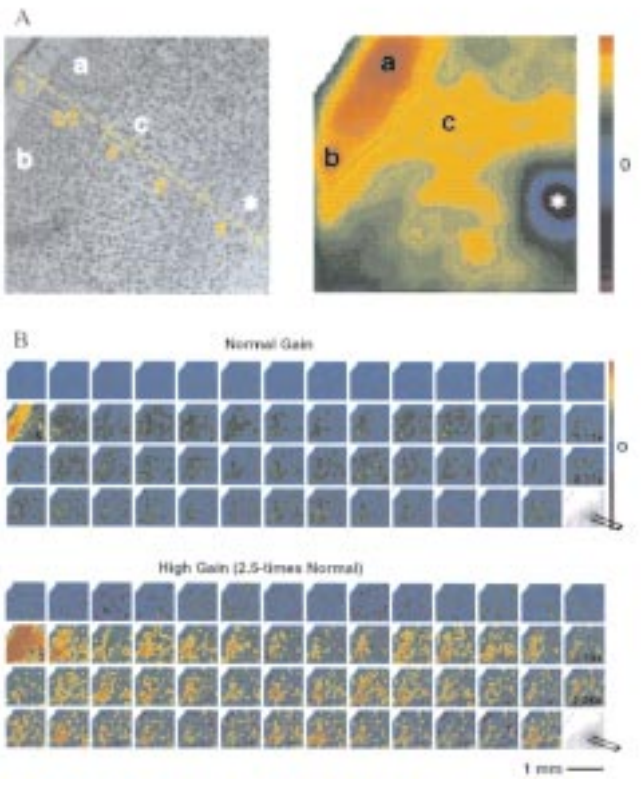

Figure 7. The fast signal shows laminar specificity while the slow signal is spatially diffuse. Depolarization corresponds to the green/yellow/red part of the false-color scale while hyperpolarization corresponds to the blue/violet scale. (*A*) Stimulation of layer 6 produces a fast signal in layers 2/3 and 4. Cresyl violet (left) and peak fluorescence responses (right) of a coronal slice from rat visual cortex, during a single-shock stimulation of layer 6 (star). Peak response appears in layer 2/3 (a,b), with a secondary focus of activation in layer 4 (c). Pseudocolor scale corresponds to $\Delta F/F = \pm 0.7\%$. (*B*) Stimulation of layer 5 produces a fast signal restricted to layers 2/3 and a slow signal that does not respect laminar boundaries. Sequence of images of the fluorescence response of a slice to a single electrical shock in layer 5. The pial surface is to the top right, the white matter at the bottom left. Top panel: the fast signal (time 0) is clearly restricted to upper layers. Scale is $\Delta F/F = \pm 1\%$. Bottom panel: the slow signal (times 0 to end) appears throughout the slice, without any clear spatial restriction. Scale is $\Delta F/F = \pm 0.4\%$.

neurons axonal terminals in layer 2/3. Nevertheless, in the neocortex an antidromic component could still be present, because the circuitry is not segregated like in CA1 (see below).

Fast Signals Have Laminar Specificity

The fast signal was stronger in specific layers above or below the stimulating electrode, whereas the slow signal extended throughout the slice, without showing any laminar specificity. For example, a single electrical stimulus delivered to layer 6 produced a fast signal in layer 2/3 and layer 4 (Fig. 7*A*,*B*). In the same experiment, however, the slow signal did not show any laminar specificity (Fig. 7*B*, lower panel). Thus, following stimulation, the slow signal appears largely as a spatially uniform depolari- zation across the slice.

Stimulating different layers produced stereotyped laminar response patterns (Fig. 8). These patterns showed little variability from trial to trial or from slice to slice. In summary, stimulation to layer 1 elicited a strong response in layer 1 and upper layer 2/3 (n = 9 slices). Stimulation of layer 2/3 produced strong responses in layer 5 and lateral layer 2/3, with smaller responses in layer 6 (n = 5 slices). Stimulation of layer 4 produced responses localized

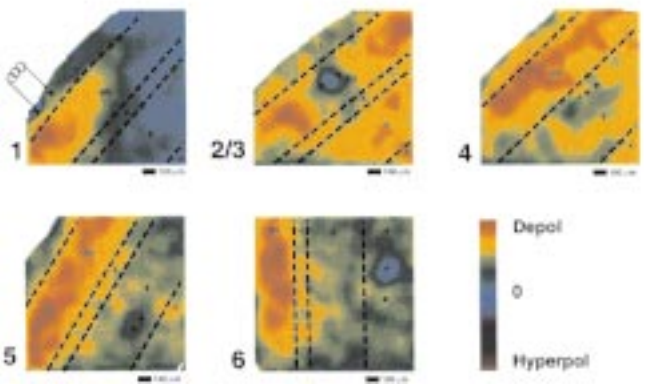

Figure 8. Laminar dependency of layer simulation experiments. Representative images from layer-specific stimulation experiments. One or two 300 μs shocks were delivered with a bipolar stimulating electrode (stars). A strong laminar specificity can be detected. Each image corresponds to the peak response, averaged over 16 experiments. Pseudocolor scales as follows: $\Delta F/F = \pm 0.22\%$ for layer 1 stimulation; $\Delta F/F = \pm 0.21\%$ for layer 2/3 stimulation; $\Delta F/F = \pm 0.22\%$ for layer 4 stimulation; $\Delta F/F = \pm 0.26\%$ for layer 5 stimulation; $\Delta F/F = \pm 0.16\%$ for layer 6 stimulation. Layer boundaries were estimated by the distance from the pial cortex as described (Materials and Methods).

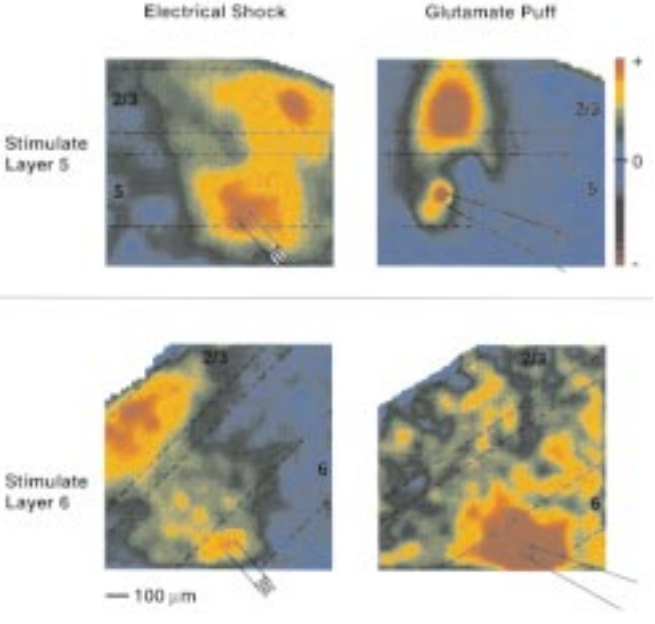

Figure 9. Glutamate pressure injections produce laminar responses. Peak responses from laminar stimulation experiments using 300 μs electrical shocks (left panels) or 3 ms glutamate puffs (right panels). Top: electrical stimulation or glutamate applications to layer 5 produce a response is layer 2/3. Bottom left: electrical stimulation to layer 6 produces a response in layer 2/3. Similar spatial patterns of response were seen in four additional slices. Bottom right: glutamate puff in layer 6, however, activates mostly layer 5 and 6. Similar spatial patterns of response, encompassing layers 4–6, were seen in three additional slices. Layer boundaries were estimated by the distance from the pial cortex. Pseudocolor scales as follows: $\Delta F/F = \pm 0.38\%$ for layer 5 electrical stimulation; $\Delta F/F = \pm 0.25\%$ for layer 5 glutamate stimulation; $\Delta F/F = \pm 0.83\%$ for layer 6 electrical stimulation; $\Delta F/F = \pm 0.20\%$ for layer 6 glutamate stimulation. The latter scale is set above saturation to emphasize the lack of activation of layers 2/3.

in layer 2/3 (n = 3 slices). Stimulation of layer 5 produced a response in layer 2/3 with a small response in layer 6 (n = 69 slices). Finally, stimulation of layer 6 produced responses in layer 4 and 2/3 (n = 7).

The laminar specificity of the fast signal may be caused by the known axonal projection patterns (Burkhalter, 1989), but could be confounded by complex pre- and postsynaptic contributions to the signals (see above). We tested if postsynaptic components of the signal were responsible for the spatial pattern of the response by repeating the layer 5 stimulation under APV/CNQX. We chose layer 5 stimulation because it gave us the largest optical responses. In 12 of 12 slice experiments (12/12) under APV/CNQX, stimulation of layer 5 produced a response largely restricted to layer 2/3, although the signal was reduced in magnitude. Similar results, i.e. no significant changes in the laminar responses from control stimulations were found with stimulations under APV/CNQX to layers 1 (4/4), layers 2/3 (4/4), layer 4 (2/2) and layer 6 (2/2). Thus, we conclude that the laminar specificity was not produced by postsynaptic responses, but rather was mediated by ortho- or antidromic presynaptic signals.

We tested if significant antidromic components were responsible for the laminar response patterns by stimulating different layers with a local perfusion of glutamate. This ensures a specific orthodromic stimulation of the pathway, as axons of passage are not stimulated by glutamate. Pressure ejection of glutamate in layer 5 produced a significant response in layer 2/3, a result identical to the electrical stimulation experiments (5/5) (Fig. 9*A*). Additional correspondence with electrical stimulation results was found when glutamate puffs were applied to layers 1, 2/3 and 4. However, in disagreement with the electrical stimulation, glutamate puffs onto layer 6 produced activation of layers 4–6, without any activation of layers 2/3 (4/4) (Fig. 9*B*; note that the color scale is saturated to accentuate the lack of response in layers 2/3).

We conclude that the laminar specificity of the fast responses were mostly due to orthodromic presynaptic signals, most likely mediated by the activation of axonal terminal fields or secondary depolarization of glia. In the case of layer 6 stimulation, however, a large superimposed antidromic activation of layer 2/3 neurons was also present. It is important to point out that all of the above experiments were carried out with the inhibitory connections intact, so part of the observed laminar specificity of the response may be refined by superimposed inhibition.

Clustered Horizontal Activation of Tangential Slices

An aspect of the cortical microcircuit that has received increased attention are the long-range horizontal projections (Gilbert and Wiesel, 1983). In cat visual cortex they are particularly prominent in the upper layers, where they can extend for several millimeters and thus span functional areas with non-overlapping receptive fields (Gilbert and Wiesel, 1983). A recent anatomical study has demonstrated a similar network of horizontal projections in the rat area 18a (Lohmann and Roerig, 1994). We wondered if we could reveal their existence optically by imaging fast signals in tangential slices cut through the upper layers. In both visual (5/5) and somatosensory cortex (4/4) we found long-range responses to extracellular electrical stimulation that were spatially heterogeneous and extended for up to 1 mm from stimulating electrode (Fig. 10).

In visual cortical slices, which encompassed areas 17 and 18a, the clusters were located ~300 μm from one another. This distance agrees with an average inter-patch distance of 250 μm for the clustered axonal projections (Lohmann and Roerig, 1994), and suggests that the clustered responses in our recordings indeed correspond to clustered horizontal projections. Peak responses in the center of the patches were ~5–10 times smaller than average responses observed with laminar stimulation experiments. The same clusters were activated with repeated stimulation of the same position in the slice and in one case the same cluster could be activated from two different stimulation sites. Finally, in an experiment with a slice that encompassed layer 4 in somatosensory cortex, stimulation of the septal region between barrels (Fig. 10*C*) produced a systematic activation of septal areas (Fig. 10*D*) (32 trials; n = 1 slice). This surprising result suggests that septal regions are preferentially connected among themselves. This idea has also been recently suggested from anatomical experiments (U. Kim and F.F. Ebner, Society for Neuroscience Abstract 49.9, 1993).

Epileptiform Activation Produces Non-modular Responses

In slices from developing neocortex clear modular units with discrete borders were discovered using calcium imaging of neuronal populations (Yuste *et al.*, 1992). We wondered if a similar modular organization was also present in the adult neocortex, and thus imaged fast VSD signals in adult slices under conditions of spontaneous activation of the circuitry, such as Mg^{2+}-free ACSF or high concentrations of the $GABA_A$ blocker bicuculline methiiodide (BMI). Both manipulations are well-known strategies to initiate epilepsy *in vitro* (Connors, 1984; Mody *et al.*, 1987; Silva *et al.*, 1991). By following the spread of the activity we investigated whether the excitability is confined to localized regions, or modules, or showed any spatial restriction that could be a reflection of structural components of the circuit.

In all experiments (BMI: n = 26 slices; Mg^{2+}-free: n = 40), the spontaneous or evoked activation of the slice produced a wave of depolarization that originated in the upper layers and then propagated laterally and vertically throughout the entire slice (Fig. 11). The speed of propagation of the front of the wave was ~1.5 mm/s, without any obvious discontinuity in any direction. Concomitant with the spread of the wave, field potentials demonstrated interictal spikes.

We conclude that under conditions where the entire slice was intrinsically active, the imaging of the wave of activity revealed a homogeneous, non-modular response. Two important caveats must be kept in mind when interpreting these results: (i) the temporal resolution of these experiments was 45–90 ms/frame, which would have averaged out spatial heterogeneities present at faster time scale; and (ii) the pharmacological methods of stimulation chosen, although intrinsic, may be very far from the precise spatio-temporal patterns of activity that stimulate the cortex *in vivo*. Nevertheless, since a similar experimental strategy revealed modular elements in developing cortex (Yuste *et al.*, 1992), the non-modularity seen here suggests that the cortical microcircuit is activated in a distributed fashion under our stimulation conditions.

Discussion

Nature of di-4-ANEPPS Signals in Neocortical Slices

In the first line of experiments we characterize the nature of the di-4-ANEPPS signal in slices by studying its spectral and temporal dependencies. We find that in response to electrical stimulation there are at least two types of signals (Fig. 2): a fast signal that peaks in tens of milliseconds and lasts for ~100 ms, and a slow signal that peaks in ~100 ms and lasts for several seconds, even in response to a single shock. The rise- and peak-time of the fast

signal follows changes in local field potential (Figs 4 and 6). Furthermore, the fast signal changes sign when the fluorescence is measured at either side of the peak in the emission spectrum (Fig. 4). These results are consistent with a major component of the fast signal being produced by an voltage-dependent behavior of the dye and thus constituting a true measurement of membrane potential. They are in agreement with previous studies using di-4-ANEPPS in bilayers, lipid vesicles, squid giant axon, mammalian heart cells, cultured mammalian neurons or invertebrate preparations (Fluhler *et al.*, 1985; Loew *et al.*, 1985; Loew *et al.*, 1992; Kleinfeld *et al.*, 1994; Rohr and Salzberg, 1994; Staub *et al.*, 1994), which we now extend to brain slices. The expected wavelength shift, however, does not prove that the fast signal is due to electrochromism, since the existence of other voltage-sensing mechanisms like solvatochromism, could contribute to the optical properties of the dye in complex ways (Fromherz and Lambacher, 1991).

The size of the fast signal (0.1–1% $\Delta F/F$ for single shock stimulation; Figs 2, 4 and 6–12) is approximately one order of magnitude smaller than previous measurements for large depolarizations with di-4-ANEPPS in bilayers (Fluhler *et al.*, 1985; Loew *et al.*, 1992) or di-8-ANEPPS in cultured myocytes (Rohr and Salzberg, 1994), although it appears similar to measurements from cultured neurons (Staub *et al.*, 1994). This reduction in the amplitude of the signal could be due to the fact that the staining of the dye is not limited to the outer leaflet of the cell membrane (Fig. 1), to the heterogeneity of the different cells stained, in particular the inclusion of glial cells, or to the lack of synchrony by the activity of the neuronal population.

The Fast Signal Has a Large Presynaptic Component and Can Be Imaged Ratiometrically

Our results demonstrate that a large fraction (~65%) of the fast signal is not affected by postsynaptic blockers (Fig. 6). This dominant signal could be mediated by three different mechanisms: (i) depolarization of presynaptic terminals of the stimulated axons or of terminals located in axonal collaterals of the stimulated ones (Grinvald *et al.*, 1982; Salzberg *et al.*, 1983); (ii) secondary depolarization of glia (Konnerth and Orkand, 1986; Lev-Ram and Grinvald, 1986) produced by axons or presynaptic terminals; and (iii) depolarization of somata and dendrites of neurons stimulated antidromically from their axons. The persistence of the signal with postsynaptic blockers and the activation of distant layers using local glutamate applications demonstrate that a presynaptic signal is present and suggest that it dominates the fast signal. A strong presynaptic component is consistent with the pattern of staining (Fig. 1) and could be caused by preferential uptake of dyes by presynaptic terminals (Betz and Bewick, 1992). Since presynaptic terminals are thought to repolarize within a few milliseconds of the arrival of the action potential (Katz, 1969), the slower decays of the fast signal isolated spectroscopically (and evident in the undershoot of Fig. 5*A* or the overshoot of Fig. 5*B*) are, however, consistent with a significant component to the voltage-sensitive signal due to persistent glial depolarization (Konnerth and Orkand, 1986). Finally, results from stimulating layer 6 (Fig. 9) indicate that an antidromic signal can also contribute to the fast signal, although the lack of activation of layer 4 with stimulation of layers 2/3 and the lack of responses in layer 5 when stimulating layer 1 suggests that antidromic activation does not play a significant role in most layer stimulation experiments. The reason why stimulation of layer 6 may particularly elicit antidromic responses is a mystery to us.

The remaining ~30% of the fast signal that is sensitive to postsynaptic blockers could be due to depolarization of postsynaptic dendrites (Grinvald *et al.*, 1982; Staub *et al.*, 1994), or to secondary presynaptic signals produced by the firing of postsynaptic neurons. This last possibility is suggested by VSD imaging of CA3 pyramidal neurons. Under 4-AP and APV/CNQX, dendrites of CA3 pyramidal neurons receive barrages of synchronous inhibitory postsynaptic potentials. However, simultaneous optical recording with photodiodes from the same dendritic fields shows synchronous depolarizing optical signals, suggesting that the optical signal is produced by depolarization of presynaptic terminals from inhibitory neurons (B. Strowbridge and D.W. Tank, unpublished observations).

The slow signal does not show wavelength dependence or follow field potential changes (Fig. 5). In unpublished studies we have found that in response to a train of stimulation the slow signal is 3–10 times larger in stained slices than in unstained slices, suggesting that the presence of the dye may serve to amplify intrinsic signals. The slow signal thus appears to have two different components: a change in scattering properties of the slice (Lipton, 1973; MacVicar and Hochman, 1991), which is evident in unstained slices in our unpublished observations; and a non voltage-sensitive behavior of the dye (Ross *et al.*, 1977), like the redistribution of dye inside cells during swelling of cellular components triggered by neuronal activity.

Local Connectivity Revealed with di-4-ANEPPS Imaging

In a second series of experiments, designed to compare our optical responses with known anatomical features of the microcircuitry, we image fast signals produced in response to weak stimulations delivered in different layers (Figs 8 and 9). Under these conditions connections from layer 4 to layer 2/3, from 2/3 to 5, from 5 to 6 and 2/3, and from 6 to 4 are detected. In addition, clustered horizontal responses in layers 2/3 are revealed (Fig. 10). Based on our studies of the nature of the signal, we propose that the spatial pattern of responses correspond to the spatial distribution of axonal projections.

Figure 10. Clustered responses revealed in tangential slices. Representative examples from experiments in tangential slices, showing clustered responses. (*A*) Experiment carried out in a tangential slice encompassing layers 2/3 from rat visual cortex. A train of 15 pulses at 10 Hz was delivered with the stimulating electrode (black dots). Patches of responsive areas located ~300 μm from one another are clearly visible. The image was created by subtracting eight stimulated from eight control movies and averaging all the frames. (*B*) Peak response of a tangential slice, cut through layers 2/3 of rat somatosensory cortex to a train of 10 shocks at 20 Hz delivered at the electrode site (black dot). Similar long-distance clustered responses are seen. (*C*) Image of a tangential slice cut through layer 4 from primary somatosensory cortex, showing clear barrels (in green) and barrel voids (in blue). The stimulating electrode is colored red. (*D*) Peak VSD response of the same slice as in (*C*) during stimulation with a single electrical shock. The response appears restricted to the septal regions, avoiding the barrels. Scale bar = 500 μm.

Figure 11. Spontaneous and evoked activation of adult slices produces a stereotyped, wave-like, response. Response of a coronal slice from visual cortex to a single 300 μs shock in the white matter, in the presence of 2 μM bicuculline methaiodide to increase excitability. Top panel: field potential and timing of frames. Bottom panel: consecutive frames are displayed in pseudocolor. The response starts in the lower layers, then extends to the upper layers and spreads laterally. The largest response occurs in layer 2/3. No clear borders or sharp spatial heterogeneities are apparent. Similar results are obtained in coronal and tangential slices in Mg^{2+}-free ACSF.

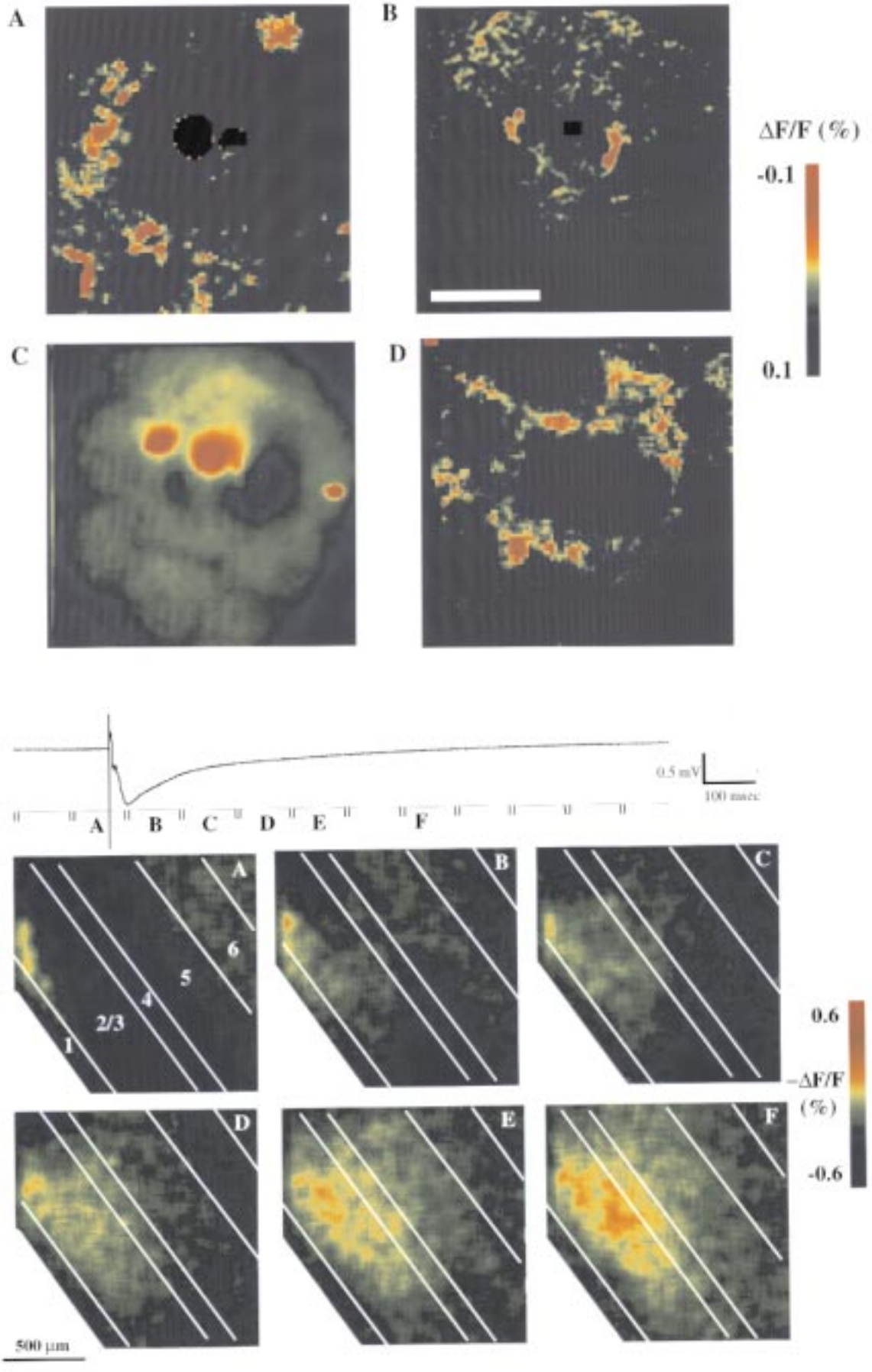
A
B
C
D
ΔF/F (%)
-0.1
0.1
0.5 mV
100 msec
A
B
C
D
E
F
A
B
C
D
E
F
6
5
4
2/3
1
0.6
-ΔF/F
(%)
-0.6
500 μm

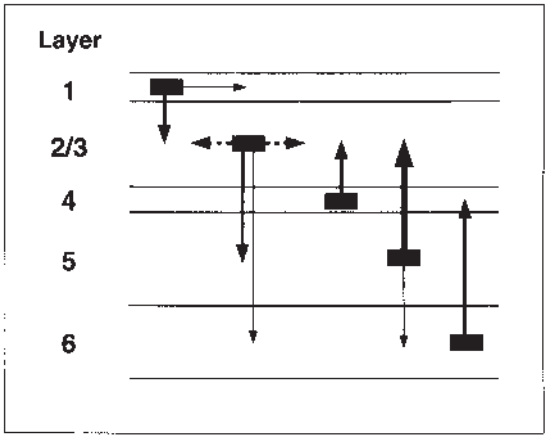

Figure 12. Proposed functional circuit diagram for rat visual cortex. This diagram summarizes all results from laminar stimulation experiments with electrical shocks or glutamate injections. Arrows extend from the stimulated layer to the layers of largest responses. The width of the arrow is proportional to the magnitude of the peak response; we constructed a 5 level scale in which the levels correspond to an peak $|\Delta F/F|$ of 0.5%, 1.0%, 1.5%, 2.0% and 2.5% (averaged over trials and different slice experiments). The strongest projections are from layers 5 and 6 to layer 2/3, and from layer 2/3 to lateral aspects of 2/3. Putative long range horizontal connections, detected in tangential slices, were weak.

Using this information we can construct a diagram of the average responses across all slices and trials (Fig. 12).

This diagram is mostly in agreement with previous anatomical studies of the 'anatomical circuit diagram' and with reports of clustered horizontal connections in cat and rat visual cortex determined with tracing techniques (Gilbert, 1983; Gilbert and Wiesel, 1983; Burkhalter, 1989; Lohmann and Roerig, 1994). We conclude that our imaging protocol is sensitive enough to reveal major circuit projections in a functional assay. In our 'functional circuit diagram' (Fig. 12), connections from layer 5 to layers 2/3 and from 2/3 to 5 are strongest, whereas distant horizontal responses are small. This may reflect differences in functional coupling between vertical and horizontal synaptic projections, as is suggested from electrophysiological studies (Hirsch and Gilbert, 1991), but could also be due to our choice of stimulation paradigm.

Lack of Modular Responses under Epileptic Activation of the Circuitry

In a third series of experiments we investigated whether there is a modular activation of the cortical microcircuit under disinhibited conditions. In spite of the clear presence of heterogeneous, laminar or clustered responses to single shocks, bath applications of bicuculline or Mg^{2+}-free ACSF induce spontaneous activations of the slice which are not restricted to any particular layer or columnar boundary and appear to propagate homogeneously through the whole slice (Fig. 11). This finding agrees with previous imaging studies of cortical and hippocampal slices under normal or disinhibited conditions (Grinvald *et al.*, 1982; Albowitz *et al.*, 1990; Albowitz and Kuhnt, 1991; Albowitz and Kuhnt, 1993; Tanifuji *et al.*, 1994; Nelson and Katz, 1995), but VSD studies in slices are complicated by the lack of single cell resolution and by the complex nature of the signal. Thus, as opposed to developing cortex, where spontaneous activation of a population of neurons with clear borders occur in slices (Yuste *et al.*, 1992), the adult cortical circuit does not seem to sustain a modular dynamic under our experimental conditions. Although more restricted responses with physiological stimulus may exist *in vivo*, the generalized spontaneous activations we image *in vitro* are consistent with a very distributed functional connectivity.

Usefulness of Voltage-sensitive Dyes for Circuit Studies

Imaging the flow of electrical activity in brain tissue stained with VSDs compliments traditional anatomical methods of studying circuits. In particular, we show that VSDs allow one to characterize the functional weight of different pathways. Further, the photobleaching and toxicity associated with di-4-ANEPPS are sufficiently small for the same slice to be imaged for up to 4 h; this may further allow for the study of plastic changes along cortical projections (e.g. Kaneko *et al.*, 1994).

The interpretation of VSD data in slices has to proceed with caution. Our results show that the signals produced by di-4-ANEPPS are complex and do not enable single-cell resolution imaging in slices. Similar limitations are expected from all currently available VSDs, although promising new strategies are being developed (González and Tsien, 1996).

A practical consequence of our demonstration of the wavelength sensitivity of the fast signal is the possibility of using dual-wavelength emission ratio measurements with VSDs in slices. As we show in Figure 4, the fast signal changes sign when measured at $\lambda = 560$ or 630 nm emission, when excited at $\lambda = 470$ nm. This wavelength dependency enables simultaneous ratio imaging, which will eliminate non-voltage components of the signal (Fig. 5), normalizes the signal for dye concentration differences across the sample, and may permit calibration of the voltage signal and estimation of the mean transmembrane potential (Montana *et al.*, 1989). An alternative approach is to image at the emission zero crossing (Figure 5*C* bottom) in order to isolate the slow, non-voltage-sensitive signal, and then subtract it from the combined signal. Both approaches could be particularly advantageous for isolating complicated non-voltage signals from recordings in the presence of continuous neuronal activity *in vivo* (Blasdel and Salama, 1986; Grinvald *et al.*, 1994; Arieli *et al.*, 1996.; Kleinfeld and Delaney, 1996).

Notes

We thank W. Denk for the two-photon imaging that led to the data in Figure 1. C.–B. Chen for the diagrams in Figure 3*B*, and A. Borst, F.F. Ebner, C. Müller, D. Orbach and D.C. Van Essen for helpful comments. R.Y. is a Sloan Research Fellow and is supported by the Klingestein, March of Dimes and EJLB Foundations.

Address correspondence to Rafael Yuste, Department of Biological Sciences, Columbia University, 1212 Amsterdam Avenue, Box 2435, New York, NY 10027, USA.

References

Albowitz B, Kuhnt U (1991) Spatio-temporal distribution of epileptiform potentials in the hippocampal slice: recordings with voltage-sensitive dyes. Eur J Neurosci 3:570–586.

Albowitz B, Kuhnt U (1993) Evoked changes of membrane potential in guinea pig sensory neocortical slices: an analysis with voltage-sensitive dyes and a fast optical recording method. Exp Brain Res 93:213–225.

Albowitz B, Kuhnt U, Ehrenreich L (1990) Optical recording of epileptiform voltage changes in the neocortical slice. Exp Brain Res 81:241–256.

Arieli, A, Sterkin, A, Grinvald, A, Aertsen, A (1996) Dynamics of ongoing activity: explanation of the large variability in evoked cortical responses. Science 273:1868–71.

Ben-Yishai R, Lev Bar-Or R, Sompolinsky H (1995) Orientation tuning by recurrent neural networks in visual cortex. Proc Natl Acad Sci USA 92:3844–3848.

Betz WJ, Bewick GY (1992) Optical analysis of synaptic vesicle recycling at the frog neuromuscular junction. Science 255:200–203.

Blasdel GG, Salama G (1986) Voltage-sensitive dyes reveal a modular organization in monkey striate cortex. Nature 321:579–585.

Burkhalter A (1989) Intrinsic connections of rat primary visual cortex: laminar organization of axonal projections. J Comp Neurol 279:171–186.

Chapman B, Zahs KR, Stryker MP (1991) Relation of cortical cell orientation selectivity to alignment of receptive fields of the geniculocortical afferents that arborize within a single orientation column in ferret visual cortex. J Neurosci 11:1347–1358.

Cinelli AR, Salzberg BM (1990) Multiple site optical recording of transmembrane voltage (MSORTV), single-unit recordings, and evoked field potentials from the olfactory bulb of the skate (*Raja erinacea*). J Neurophys 64:1767–1790.

Connors B (1984) Initiation of synchronized neuronal bursting in neocortex. Nature 310: 685–687.

Crick FHC, Asanuma C (1986) Certain aspects of the anatomy and physiology of the cerebral cortex. In: Parallel distributed processing (McClelland JL, Rumelhart DE, eds), pp 333–371. Cambridge, MA: MIT Press.

Denk W, Delaney KR, Gelperin A, Kleinfeld D, Strowbridge BW, Tank DW, Yuste R (1994) Anatomical and functional imaging of neurons using 2-photon laser scanning microscopy. J Neurosci Methods 54:151–162.

Denk W, Strickler JH, Webb WW (1990) Two-photon laser scanning fluorescence microscopy. Science 248:73–76.

Douglas RJ, Koch C, Mahowald M, Martin KAC, Suarez HH (1995) Recurrent excitation in neocortical circuits. Science 269:981–985.

Fluhler E, Burnham VG, Loew LM (1985) Spectra, membrane binding and potentiometric responses of new charge shift probes. Biochemistry 24:5749–5755.

Fromherz P, Lambacher A (1991) Spectra of voltage-sensitive fluorescence of styryl-dye in neuron membrane. Biochim Biophys Acta 1068:149–56.

Georgopoulos AP, Lurito JT, Petrides M, Schwartz AB, Massey JT (1989) Mental rotation of the neuronal population vector. Science 243:234–236.

Gilbert CD (1983) Microcircuitry of visual cortex. Annu Rev Neurosci 6:217–247.

Gilbert CD, Wiesel TN (1979) Morphology and intracortical projections of functionally characterised neurons in the cat visual cortex. Nature 280:120–125.

Gilbert CD, Wiesel TN (1983) Clustered intrinsic connections in cat visual cortex. J Neurosci 3:1116–1133.

Gilbert CD, Wiesel TN (1985) Intrinsic connectivities and receptive field properties in visual cortex. Vis Res 25:365–374.

González JE, Tsien RY (1996) Voltage sensing by fluorescence resonance energy transfer in single cells. Biophys J 69:1272–1280.

Grinvald A, Frostig RD, Lieke E, Hildesheim R (1988) Optical imaging of neuronal activity. Physiol Rev 68:1285–1365.

Grinvald A, Lieke EE, Frostig RD, Hildesheim R (1994) Cortical-point-images and long-range lateral interaction revealed by real-time optical imaging of macaque monkey primary visual cortex. J Neurosci 14:2545–2568.

Grinvald A, Manker A, Segal M (1982) Visualization of the spread of electrical activity in rat hippocampal slices by voltage-sensitive optical probes. J Physiol 333:269–291.

Hirsch JA, Gilbert CD (1991) Synaptic physiology of horizontal connections in the cat's visual cortex. J Neurosci 11:1800–1809.

Hopfield JJ (1982) Neural networks and physical systems with emergent collective computational abilities. Proc Natl Acad Sci USA 79:2554–2558.

Hopfield JJ, Tank DW (1986) Computing with neural circuits: a model. Science 233:625–633.

Hubel DH, Wiesel TN (1977) Functional architecture of the macaque monkey visual cortex. Proc R Soc Lond B 198:1–59.

Kaneko,T, Carla, MA and Asanuma, H (1994) Information processing within the motor cortex. II. Intracortical connections between neurons receiving somatosensory cortical input and motor output neurons of the cortex. J Comp Neurol 345:172–184.

Katz B (1969) The release of neurotransmitter substances. Liverpool: Liverpool University Press.

Kleinfeld D, Delaney KR (1996) Distributed representation of vibrissa movement in the upper layers of somatosensory cortex revealed with voltage-sensitive dyes. J Comp Neurol 375:89–108 (erratum 378:594).

Kleinfeld D, Delaney KR, Fee MS, Flores GA, Tank DW, Gelperin A (1994) Dynamics of propagating waves in a terrestial molusc: an electrical and optical study. J Neurophysiol 721402–1419.

Konnerth A, Orkand RK (1986) Voltage-sensitive dyes measure potential changes in axons and glia of the frog optic nerve. Neurosci Lett 66:49–54.

Konnerth A, Obaid AL, Salzberg BM (1987) Optical recording of electrical activity from parallel fibres and other cell types in skate cerebellar slices *in vitro*. J Physiol 393:681–702.

Langdon RB, Sur M (1990) Components of field potentials evoked by white matter stimulation in solated slices of primary visual cortex: spatial distribution and synaptic order. J Neurophysiol 64:1484–1501.

Lev-Ram V, Grinvald A (1986) Ca^{2+}- and K^{+}-dependent communication between central nervous myelinated axons and oligodendrocytes revealed by voltage-sensitive dyes. Proc Natl Acad Sci USA 83: 6651–6655.

Lipton P (1973) Effects of membrane depolarization on light scattering by cerebral cortical slices. J Physiol 231:365–383.

Loew LM, Cohen LB, Dix J, Fluhler EN, Montana V, Salama G, Jian-Young W (1992) A naphthyl analog of the aminostyryl pyridinium class of potentiometric membrane dyes shows consistent sensitivity in a variety of tissue, cell and model membrane preparations. J Membr Biol 130:1–10.

Loew LM, Cohen LB, Salzberg BM, Obaid AL, Bezanilla F (1985) Charge shift probes of membrane potential. Characterization of aminostyrylpyridinium dyes on the squid giant axon. Biophys J 47:71–77.

Loew LM, Scully S, Simpson L, Waggonner AS (1979) Evidence for a charge-shift electrochromic mechanism in a probe for membrane potential. Nature 281:497–499.

Lohmann H, Roerig B (1994) Long-range horizontal connections between supragranular pyramidal cells in the extrastriate visual cortex of the rat. J Comp Neurol 344:543–558.

MacVicar BA, Hochman D (1991) Imaging of synaptically evoked intrinsic optical signals in hippocampal slices. J Neurosci 11:1458–1469.

Mody I, Lambert JDC, Heinemann U (1987) Low extracellular magnesium induces epileptiform activity and spreading depression in rat hippocampal slices. J Neurophysiol 57:869–888.

Montana V, Farkas DL, Loew LM (1989) Dual-wavelength ratiometric fluorescence measurements of membrane potential. Biochemistry 28:4536–4539.

Mountcastle VB (1982) An organizing principle of cerebral function: the unit module and the distributed system. In: The mindful brain (Schmitt HO, ed.), pp 1–50. Cambridge, MA: MIT Press.

Nelson DA, Katz LC (1995) Emergence of functional circuits in ferret visual cortex visualized by optical imaging. Neuron 15:23–34.

Platt JR (1956) Electrochromism, a possible change of color producible in dyes by an electric field. J Chem Phys 25:80–105.

Rohr S, Salzberg BM (1994) Multiple site optical recording of transmembrane volatge (MSORTV) in petterned growth heart cell cultures: assesing electrical behaviour, with microsecond resolution, on a cellular and subcellular scale. Biophys J 67:1301–1315.

Ross WN, Salzberg LB, Cohen LB, Grinvald A, Davila HV, Waggoner AS, Wang C-H (1977) Changes in absorption, fluorescence, dichroism, and birefringence in stained giant axons: optical measurements of membrane potential. J Membr Biol 33:141–183.

Salzberg B, Obaid A, Senseman D, Gainer H (1983) Optical recording of action potentials from vertebrate nerve terminals using potentiometric probes provides evidence for sodium and calcium components. Nature 306:36–40.

Salzberg BM, Obaid AL, Gainer H (1985) Large and rapid changes in light scattering acompany secretion by nerve terminals in the mammalian neurohypophysis. J Gen Physiol 86:395–411.

Silva LR, Amitai Y, Connors B (1991) Intrinsic oscillation of neocortex generated by layer 5 pyramidal neurons. Science 251:432–435.

Somers DC, Nelson SB, Sur M (1995) An emergent model of orientation selectivity in cat visual cortical simple cells. J Neurosci 15:5448–5465.

Sompolinsky H, Golomb D, Kleinfeld D (1991) Cooperative dynamics in visual processing. Phys Rev A 43:6990–7011.

Staub C, De Schutter E, Knoepfel T (1994) Voltage-imaging and simulation of effects of voltage- and agonists-activated conductances on soma–dendritic voltage coupling in cerebellar Purkinje cells. J Comput Neurosci 1:301–311.

Swindale NV (1990) Is the cerebral cortex modular? Trends Neurosci 13:487–492.

Tanifuji M, Sugiyama T, Murase K (1994) Horizontal propagation of excitation in rat visual cortical slices revealed by optical imaging. Science 266:1057–1059.

Yuste R (1994) Calcium imaging of cortical circuits in slices of developing neocortex. In: Enabling technologies for cultured neural networks (Stenger D, McKenna T , ed.), pp 207–234. San Diego: Academic Press.

Yuste R, Peinado A, Katz LC (1992) Neuronal domains in developing neocortex. Science 257:665–669.

Zilles K, Wree A (1985) Cortex: areal and laminar structure. In: The rat nervous system (Paxinos G, ed.), pp 375–415. Sydney: Academic Press.